Measurement of the $n=9$ F-to-G intervals in atomic lithium

C. H. Storry, N. E. Rothery, and E. A. Hessels
York University, 4700 Keele Street, Toronto, Ontario, Canada
(Received 16 May 1996)

The $n=9$ F-to-G intervals in atomic lithium are measured to a precision of 1 ppm. These transitions are driven using microwaves in a Ramsey-separated-oscillatory-field configuration. The results are 1920.6767(22) and 1928.7221(22) MHz for the $9F_{7/2}$-to-$9G_{9/2}$ and $9F_{5/2}$-to-$9G_{7/2}$ intervals, respectively. These are the most accurate measurements of any fine-structure intervals in Rydberg states of the lithium atom. [S1050-2947(96)05610-7]

PACS number(s): 32.30.Bv

INTRODUCTION

High-precision measurements of the fine-structure intervals of atoms have led to many important tests of physics. Initially, such tests were restricted to excited states of atomic hydrogen since hydrogen was the only atom for which high-precision calculations of the energy intervals could be performed. Measurements of fine-structure intervals using atomic beams have verified relativistic, nuclear-mass, nuclear-size, anomalous-electron-magnetic-moment, Lamb-shift, and other effects in the hydrogen atom.

The two-electron atom cannot be solved analytically, and thus high-precision calculations of helium fine-structure intervals (energy intervals between states with the same principal quantum number n and different orbital angular momentum L) are more difficult to obtain. States which have one of the electrons excited to a high-n, high-L state, however, have wave functions which are more easily calculated since both electrons have nearly hydrogenic wave functions, with the inner electron in a $1S$ state about the $Z=2$ nucleus and the outer electron in an nL state about the $Z=1$ core (nucleus plus $1S$ electron) of the atom. Corrections to this hydrogenic approximation can be obtained by calculating the dipole polarizability (and higher-order polarizabilities) [1] of the He^+ $1S$ wave function, and the associated effects on the nL wave function. Relativistic corrections to these polarization energies [2,3] can also be calculated. High-precision measurements [4] of the helium Rydberg fine structure have provided tests of the relativistic, radiative, and retardation (Casimir) effects on the large distance scale (approximately $100a_0$) of these atoms. Very precise variational calculations of helium energies [5] are now available for the entire singly excited series of states (up to $n=10$). These calculations essentially solve this two-electron atom and thus bring the theoretical understanding of the helium atom to almost the same level as that of atomic hydrogen. These calculations can be compared to high-precision fine-structure measurements of low-lying states [6] as well as the Rydberg fine-structure measurements [4]. Discrepancies between theory and experiment in the latter remain as an outstanding problem in atomic physics.

Recently, progress has also been made on precision calculations of the three-electron atom. Again, states with one electron excited up to a Rydberg state are simpler, since the outer electron is then in a nearly hydrogenic orbit and the two-electron core has wave functions which are very nearly heliumlike. Calculations of the fine structure of Rydberg states of lithium have been obtained using polarizabilities [7] (including recently calculated relativistic corrections to the Li^+ dipole polarizability [8]). Precise variational calculations of the lower-energy levels [9] have also been done. Neither the variational calculations nor the polarization calculations are yet at the precision of those in helium, but both are continuing to be improved and extended [10,11]. We present here the most precise of any measurements of Rydberg fine-structure intervals [12] in the three-electron atom. These measurements of the lithium-7 $n=9$ F-to-G ($L=3$ to 4) fine-structure intervals are at an accuracy of 1 ppm, which is 500 times more accurate than previous measurements [13] of these intervals. They will, with the expected improvements in theory, be used to provide precision tests of the physics (including relativistic, radiative, and retardation effects) of the three-electron atom. The results can also be used as input data to high-precision calculations of Stark shifts in Rydberg states of lithium, which have recently been used [14] to measure electric fields to an accuracy of 2 ppm.

EXPERIMENTAL TECHNIQUE

The experimental setup is similar in many ways to that of a previous separated-oscillatory-field (SOF) measurement of the $n=10$ $^+F_3$-to-$^+G_4$ interval in helium [15]. A schematic of the experiment is shown in Fig. 1. Lithium-7 ions of 3.5, 5.5, or 7.5 keV are formed in a Colutron ion source. The ion source is modified as it was in the experiment of Ref. [16] to allow for longer uninterrupted operation. The ions are neu-

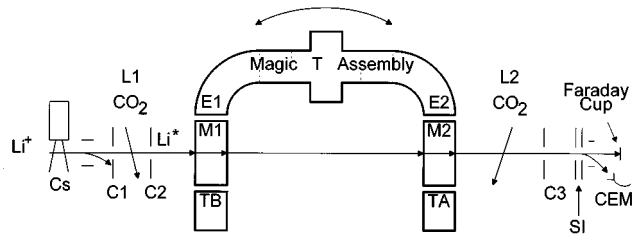

FIG. 1. Schematic of the experimental setup. Details of the setup are given in the text, with further details given in Ref. [15].

tralized via charge exchange with a dense thermal beam of atomic cesium. The lithium ions which are not neutralized in the cesium target are deflected out of the beam, while the neutral lithium atoms, some of which are in $n=9$ Rydberg states, continue along the beamline. The cross section and the direction of the neutral lithium beam is determined by three collimators ($C1$, $C2$, and $C3$ of Fig. 1). At $L1$ in Fig. 1, $9F$ lithium atoms are transferred into the $19G$ state by a $^{12}C^{18}O_2$ laser which is tuned to the $IIP(42)$ line at 9.517 μm. Fine tuning of this laser frequency is accomplished by varying the angle between the laser beam and the fast lithium beam, and thus varying the Doppler shift of the laser frequency.

After $L1$, there is a large population difference between the $9F$ and $9G$ states, and a transition between these two states is driven by microwave fields at $M1$ and $M2$ in Fig. 1. $M1$ and $M2$ are two sections of WR430 waveguide which are set up in a separated-oscillatory-field configuration. These waveguide sections have 0.4×0.8-in. holes through which the atomic beam passes and are aligned to be perpendicular to the atomic beam (to within 0.3 mrad) using a high-power surveyor's scope. The microwaves are generated by an Anritsu model MG3602A signal generator which derives its timebase reference (accurate to 10^{-11}) from a Stelar model 100B satellite connection to the global positioning system (GPS). The microwaves are switched between the E and H input ports of a Struthers M352M Magic-T, the two outputs of which are connected to the two waveguide sections $M1$ and $M2$. When the H input is used, the microwaves in $M1$ and $M2$ are nearly in phase; when the E input is used, they are approximately 180° out of phase. After passing $M1$ and $M2$, the microwaves are terminated using Struthers model 200M precision waveguide terminators, which have reflections of $|\Gamma|\approx0.025$.

After passing through the microwave fields, the atoms are intersected by a second CO_2 laser beam (at $L2$ in Fig. 1). This laser beam is Doppler tuned to excite the $9G$-to-$19H$ transition and is used to determine what fraction of the $9G$ atoms made the $9G$-to-$9F$ transition in the microwave region. The $n=19$ atoms are then Stark ionized in an electric field of 9 kV/cm (at SI in Fig. 1), and the resulting ions are deflected into a Channeltron electron multiplier (CEM) detector. The signal from the CEM is directed into a current amplifier followed by a lock-in amplifier which extracts the component which is synchronous with the switching of the microwaves between the E and H ports of the Magic T. This signal is sent to a computer for storage and analysis. The remainder of the neutral lithium beam continues through the Stark-ionization region and is monitored on a Faraday cup.

MEASUREMENTS

Both the $9F_{7/2}$-to-$9G_{9/2}$ and the $9F_{5/2}$-to-$9G_{7/2}$ intervals are measured. These two transitions are separated by approximately 8 MHz, and are well resolved in the measurement. The much smaller hyperfine structure is totally unresolved. Data are taken at three beam speeds (3.5, 5.5, and 7.5 keV). Half of the data are taken with the Magic T above $M1$ and $M2$ (as shown in Fig. 1, with the microwaves propagating downward) and the other half are taken with the Magic T below and the microwaves propagating upward. Also, half of the data are taken with the orientation of the Magic T reversed as indicated by the arrow in Fig. 1. When doing these reversals, the waveguide bends ($E1$ and $E2$) remain securely fastened to the Magic T, and this whole Magic-T assembly is reoriented. The geometry of the Magic-T assembly and of $M1$ and $M2$ (which remain securely fastened in place throughout the measurements) are constructed to tolerances of 0.001 in. or better so that the Magic-T assembly can be connected (using precision dowel pin connections) to $M1$ and $M2$ in all four orientations.

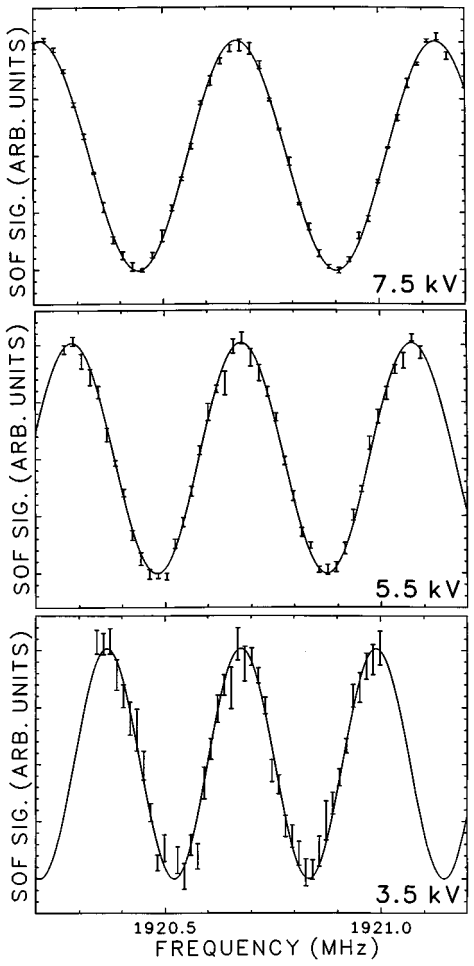

FIG. 2. Observed separated-oscillatory-field line shape near the center of the $9F_{7/2}$-to-$9G_{9/2}$ resonance. The data are the average of data taken in several separate scans of the resonance. Data are shown for the three beam speeds. The solid lines are fits to a simple cosine line shape.

The data consist of several scans taken on each of the two resonances at each of the three beam speeds and in each of the four orientations of the Magic T. After completion of this entire set of data, the set is repeated (except for one of the orientations of the Magic T which is missing in the second data set). In all, 150 h of data are taken.

Typical signals are plotted as a function of frequency in Fig. 2. The expected line shape for these signals is the Ramsey-separated-oscillatory-field line shape, which consists of Ramsey oscillations within a Rabi envelope. The line shape can be approximated using time-dependent perturbation theory, which predicts

TABLE I. Line centers for the two measured intervals. The first column gives the orientation of the Magic-T assembly. ''Reversed'' indicates the reversal shown by the arrow in Fig. 1. The second column shows the location of the Magic-T assembly (''Top'' indicates that the microwaves are traveling downward). The third column gives the acceleration potential of the ion beam. The final two columns give the average line centers for the two measured transitions. These values include all of the systematic corrections and uncertainties from Table II, except for the uncertainty associated with the unresolved hyperfine structure. The final two rows give the average of the line centers obtained in the 12 experimental configurations, with the final row including the 2.0-kHz uncertainty due to the unresolved hyperfine structure. The line centers are given in MHz, with one-standard-deviation uncertainties given in parentheses.

Magic-T orientation	Magic-T location	Acceleration potential (kV)	$9F_{7/2}$-$9G_{9/2}$ (MHz)	$9F_{5/2}$-$9G_{7/2}$ (MHz)
Normal	Top	7.5	1920.6781(18)	1928.7234(20)
	Bottom	7.5	1920.6803(18)	1928.7283(20)
	Top	5.5	1920.6799(25)	1928.7248(25)
	Bottom	5.5	1920.6805(20)	1928.7244(21)
	Top	3.5	1920.6771(31)	1928.7226(37)
	Bottom	3.5	1920.6792(25)	1928.7263(27)
Reversed	Top	7.5	1920.6718(19)	1928.7209(22)
	Bottom	7.5	1920.6742(18)	1928.7179(16)
	Top	5.5	1920.6741(21)	1928.7184(21)
	Bottom	5.5	1920.6757(23)	1928.7180(24)
	Top	3.5	1920.6739(22)	1928.7221(22)
	Bottom	3.5	1920.6755(22)	1928.7180(22)
Average of all configurations			1920.6767(10)	1928.7221(10)
Average including hyperfine uncertainty			1920.6767(22)	1928.7221(22)

$$\left(\frac{2V}{h(f-f_0)}\sin[\pi\tau(f-f_0)]\right)^2\cos[2\pi T(f-f_0)], \quad (1)$$

where f is the microwave frequency, f_0 is the resonant frequency of the transition, T is the time it takes the atoms to travel from the center of $M1$ to the center of $M2$ [a distance of 98.095(25) cm], τ is the time the atoms spend in each of the microwave regions [a distance of 5.461(7) cm], $V=eE_\mu z_{FG}$ is the dipole matrix element for the transition, E_μ is the amplitude of the microwave field, and z_{FG} is the z matrix element between the two states. In the present measurements, the beam speeds are $\beta_{3.5\ \mathrm{kV}}=0.001\,03$, $\beta_{5.5\ \mathrm{kV}}=0.001\,29$, and $\beta_{7.5\ \mathrm{kV}}=0.001\,51$, which lead to T's and τ's of $T_{3.5\ \mathrm{kV}}=3.18\ \mu$s, $T_{5.5\ \mathrm{kV}}=2.54\ \mu$s, $T_{7.5\ \mathrm{kV}}=2.17\ \mu$s, $\tau_{3.5\ \mathrm{kV}}=0.177\ \mu$s, $\tau_{5.5\ \mathrm{kV}}=0.141\ \mu$s, and $\tau_{7.5\ \mathrm{kV}}=0.121\ \mu$s. The τ's lead to Rabi widths of 5.65, 7.08, and 8.29 MHz for the three beam speeds and the T's yield intervals of 0.157, 0.197, and 0.230 MHz between the zeroes of the Ramsey oscillations (see Fig. 2). As discussed in Ref. [15], the line shape near the line center (even when the simplifying assumptions of time-dependent perturbation theory are not used) is approximated well by a simple cosine function. Thus data such as those shown in Fig. 2 are fit to a simple cosine function to extract the resonant frequency of the atomic transition. Several systematic corrections must be applied to the centers obtained from the fits. Table I shows the averaged results of fits of the data taken in each of the experimental configurations. The values in that table include the systematic corrections shown in Table II.

One important systematic effect results from the relative microwave phase in the two microwave interaction regions ($M1$ and $M2$). Ideally, the relative phase is either 0° or 180°, but nonidealities in the Magic T, or mismatched lengths in $E1$ and $E2$, could cause the relative phase at the outputs of $E1$ and $E2$ to be shifted. However, the shift due to this phase mismatch changes sign when the orientation of the Magic-T assembly is reversed (as shown by the arrow in Fig. 1), and thus the average of centers taken in these two orientations is independent of effects due to this phase mismatch. The average difference between line centers obtained in the two orientations (see Table I) is 5 kHz, indicating that the phase mismatch is approximately 3°.

A second mechanism which shifts the relative phase is the direction of the atomic beam. If the beam passes through the second microwave region at a different vertical position than it did through the first region, a shift in the relative phase will result. The sign of this shift is reversed when the direction of microwave propagation is reversed. Thus when centers obtained with the Magic-T assembly on the top and on the bottom of $M1$ and $M2$ are averaged, this relative phase effect is canceled.

Another systematic effect which depends on the direction of the atomic beam is the first-order Doppler shift of the microwave frequency. This effect is also canceled when the average is taken of centers obtained with the microwaves propagating in the two directions. The fact that on average the data taken with the Magic-T assembly on top differ by only 1 kHz from the data taken with it on the bottom, indicates that the direction of the beam (on average) is within 0.2 mrad of perpendicular to the microwave propagation in $M1$ and $M2$.

Since the focusing and deflection of the ion beam are adjusted during each data run, it is possible that the direction of the beam varies slightly from one data run to another. The

TABLE II. Systematic effects and uncertainties. Statistical uncertainties are the one-standard-deviation uncertainties in the mean of all data taken for each of the measured intervals.

	Correction (kHz)	Uncertainty (kHz)
Statistical uncertainty from fits		0.4
Statistical uncertainty due to variation in beam direction		0.5
Time dilation	+2.2, +1.6, +1.0[a]	0.0
dc Stark shift	+0.6	0.6
Neighboring resonances		0.5
ac Stark shift	+0.1	0.0
Blackbody radiation shift	−0.2	0.1
Terminator reflections	−0.3, −0.3, −0.2[a]	0.1
Unresolved hyperfine structure		2.0
Total uncertainty		2.2

[a]Corrections for 7.5-, 5.5-, and 3.5-keV beam energies.

extent of such variations is limited by collimators $C1$ and $C3$, which have heights of 0.041 and 0.120 in. and which are separated by 1.50 m. The estimated deviation of the beam direction from day to day is ± 0.5 mrad, which leads to frequency shifts (due to a combination of relative phase shifts and first-order Doppler shifts) of 2.2 kHz. Due to this possible variation, a statistical uncertainty of this size is included in each of the data runs for each of the measurements, and the effect of this statistical uncertainty on the mean of all of the data runs is included in the second row of Table II.

Time dilation (or second-order Doppler) shifts of $\frac{1}{2}\beta^2 f$ are present in the measurements, and the values in Table I include corrections of 2.2, 1.6, and 1.0 kHz for the 7.5-, 5.5-, and 3.5-keV atomic beams. The beam speeds are very accurately determined from the accelerating potential, and thus the uncertainty in this correction is less than 0.1 kHz.

dc Stark shifts due to stray electric fields in the microwave regions are a major concern. The helium 20^3D-to-20^3F transition, which has a Stark-shift rate which is 100 times larger than that of the measured intervals, is used to monitor the stray fields. The position of the helium interval is measured three times over the three-month period of the experiment and indicates that rms dc electric fields of approximately 12 mV/cm are present. Since the Stark-shift rate of the $9F$-to-G intervals is -4.2 MHz/(V^2/cm^2), this leads to Stark shifts of 0.6 kHz for the measured intervals. Since the field monitor uses a helium rather than lithium beam and since the fields (which are at least partially due to surface charging effects) might be slightly different for the two beams, a conservative estimate of ± 0.6 kHz is made for the uncertainty in this correction, as shown in Table II.

Another concern is that a slight overlap between the two resonant features, which are separated by approximately 8 MHz, might lead to small shifts in the measured line centers. If such shifts exist, they would be very dependent on the beam speed since both the Rabi envelope and the Ramsey oscillations depend on the speed of the atoms. Since data taken at three different beam speeds lead to centers that agree at the ± 0.5-kHz level of precision on both of the resonances, we conclude that the effect of overlap is small. We include an uncertainty of 0.5 kHz for this effect in Tables I and II.

Several other small corrections are ac Stark shifts due to blackbody radiation, ac Stark shifts due to the applied microwaves, and a relative phase shift caused by reflections off of the microwave terminators. These corrections are all small compared to the uncertainty of the present measurement, but are included in Table II for completeness. The first is calculated using the formalism of Farley and Wing [17] and the latter two are calculated as described in Ref. [15].

The centers (for each of the experimental configurations) corrected for the systematic effects described above are shown in Table I. The average values are given in the second last row of the table. One additional uncertainty must be applied to these measured values, namely, the uncertainty associated with the unresolved hyperfine structure. The hyperfine components of this transition are within ± 7 kHz of the frequency at which the resonance would be if no hyperfine structure were present. If these components are all statistically weighted (i.e., all levels are equally populated and all transitions are driven equally), there is no effect on the line center. We believe this to be, in fact, the case for the present measurement. However, since we have no direct measure of the relative populations of the unresolved hyperfine states, we include an uncertainty of ± 2.0 kHz, which is a conservative estimate of the effect of unequal populations in the hyperfine levels. The final row in Table I gives the final measured values, including this uncertainty.

DISCUSSION OF RESULTS

The results can be compared to earlier measurements [13] of Cooke *et al.*, which were obtained in a thermal beam using laser excitation and observing changes in fluorescence as one-photon D-to-F and two-photon D-to-G microwave transitions are driven. The difference between the D-to-F and D-to-G intervals gives measurements of the F-to-G intervals as shown in the first row of Table III. These measurements are slightly higher (1.9 standard deviations) than the present measurements which are shown in the second row, and which are 500 times more precise.

The only theoretical prediction for the energy interval comes from the polarization model calculations of Drachman and Bhatia. The $9F$-to-$9G$ interval of 1935 ± 27 MHz, which is obtained using their prescription [7], including the

TABLE III. Comparison of present measurements to previous measurements and theory. Frequencies are given in MHz, with one-standard-deviation uncertainties in the last digits given in parentheses. The column labeled ''Average'' gives the average of the two intervals, and the last column gives the splitting between the two measured frequencies.

	$9F_{7/2}$-$9G_{9/2}$	$9F_{5/2}$-$9G_{7/2}$	Average	Difference
Prev. expt.[a]	1922.6 (10)	1930.7 (10)	1926.6 (10)	8.1 (14)
Present expt.	1920.6767 (22)	1928.7221 (22)	1924.6994 (22)	8.0454 (31)
Theory			1935 (27)[b]	8.029[c]

[a]Reference [13].
[b]Calculated using the prescription of Drachman and Bhatia, Ref. [7].
[c]Hydrogenic approximation of spin-orbit contribution.

lowest-order relativistic correction and the second-order dipole-polarizability correction Δ_2 which is calculated according to the formula of Drake and Swainson [18], is in good agreement with the present measurement. Much more accurate energy predictions will be necessary in order to make a meaningful comparison with the present experimental result.

The frequency difference between the two measured intervals is predominantly due to the spin-orbit interaction. The measured splitting is 8.0454(31) MHz, which is slightly larger than the hydrogenic prediction of 8.029 MHz obtained from the spin-orbit formula:

$$\Delta E_{\mathrm{SO}}=\frac{-\alpha^2 R(1+\alpha/\pi)}{n^3(j+1/2)}, \tag{2}$$

where R is the Rydberg constant, α is the fine-structure constant, and the factor of $(1+\alpha/\pi)$ includes (to lowest order) the effect of the anomalous moment of the electron. The difference of 16 kHz from the hydrogenic prediction is not surprising since similar splittings in helium show similar differences from hydrogenic predictions. The splitting [5] between the 10^3F_4-to-10^3G_5 and the 10^3F_2-to-10^3G_3 intervals in helium, for example, differs from the hydrogenic prediction [19] by more than 20 kHz. The nonhydrogenic contributions are due primarily to the penetration of the $10F$ wave function into the core of the atom [19] and the distortion of the $10F$ and $10G$ wave functions which results from the polarization of the core. No calculation of these nonhydrogenic effects presently exists for Rydberg states of lithium.

One application for the present measurements is as input data for the precision calculation of Stark shifts in Rydberg states of lithium [14], which have recently been applied in making measurements of electric fields at an unprecedented precision of 2 ppm. These calculations require precise values for the quantum defects of lithium Rydberg states, and the present measurement, when combined with polarization calculations for the $9G$ states, provides significantly higher-precision values for the defects of the $9F$ states.

The present measurements are the most precise of any fine-structure measurements in Rydberg states of lithium. They will form a strong test of the physics of this three-electron atom when expected theory for these states becomes available.

ACKNOWLEDGMENTS

This work was supported by the Natural Sciences and Engineering Research Council of Canada. The authors wish to acknowledge helpful conversations with Richard Drachman.

[1] Richard J. Drachman, Phys. Rev. A **26**, 1228 (1982).
[2] Richard J. Drachman, Phys. Rev. A **31**, 1253 (1985); **38**, 1659(E) (1988).
[3] E. A. Hessels, Phys. Rev. A **46**, 5389 (1992).
[4] E. A. Hessels, F. J. Deck, P. W. Arcuni, and S. R. Lundeen, Phys. Rev. Lett. **65**, 2765 (1990); **66**, 2544 (1991); E. A. Hessels, P. W. Arcuni, F. J. Deck, and S. R. Lundeen, Phys. Rev. A **46**, 2622 (1992); N. E. Claytor, E. A. Hessels, and S. R. Lundeen, *ibid*. **52**, 165 (1995); and Ref. [15].
[5] G. W. F. Drake, in *Long Range Casimir Forces: Theory and Recent Experiments in Atomic Systems*, edited by F. S. Levin and D. Micha (Plenum, New York, 1993); G. W. F. Drake and Z. C. Yan, Phys. Rev. A **46**, 2378 (1992).
[6] D. Shiner, R. Dixson, and P. Zhao, Phys. Rev. Lett. **72**, 1802 (1994).
[7] A. K. Bhatia and R. J. Drachman, Phys. Rev. A **45**, 7752 (1992); R. J. Drachman and A. K. Bhatia, *ibid*. **51**, 2926 (1995).
[8] W. R. Johnson and K. T. Cheng, Phys. Rev. A **53**, 1375 (1996).
[9] Z.-C. Yan and G. W. F. Drake, Phys. Rev. A **52**, 3711 (1995).
[10] Gordon W. F. Drake (private communication).
[11] Richard J. Drachman (private communication).
[12] For a review of atomic lithium measurements, including fine structure, see L. J. Radziemski, R. E. Engleman, Jr., and J. W. Brault, Phys. Rev. A **52**, 4462 (1995).
[13] W. E. Cooke, T. F. Gallagher, R. M. Hill, and S. A. Edelstein, Phys. Rev. A **16**, 1141 (1977).
[14] G. D. Stevens, C.-H. Iu, T. Bergeman, H. J. Metcalf, I. Seipp, K. T. Taylor, and D. Delande, Phys. Rev. Lett. **75**, 3402 (1995); Phys. Rev. A **53**, 1349 (1996).
[15] C. H. Storry, N. E. Rothery, and E. A. Hessels, Phys. Rev.

Lett. **75**, 3249 (1995); Phys. Rev. A (to be published).
[16] N. E. Rothery, C. H. Storry, and E. A. Hessels, Phys. Rev. A **51**, 2919 (1995).
[17] J. W. Farley and W. H. Wing, Phys. Rev. A **23**, 2397 (1981).
[18] G. W. F. Drake and R. A. Swainson, Phys. Rev. A **44**, 5448 (1991).
[19] E. A. Hessels, W. G. Sturrus, S. R. Lundeen, and D. R. Cok, Phys. Rev. A **35**, 4489 (1987).